Journal of Solid State Chemistry 199 (2013) 160–163

Contents lists available at SciVerse ScienceDirect

Journal of Solid State Chemistry

journal homepage: www.elsevier.com/locate/jssc

Nickel segment-length dependent magnetic properties of Au–Ni–Au nanowires at low temperature fabricated by electrochemical deposition

S. Ishrat [a], K. Maaz [a,c], Kyu Joon Lee [b], Myung-Hwa Jung [b], Gil-Ho Kim [a,*]

[a] School of Electronic and Electrical Engineering and Sungkyunkwan Advanced Institute of Nanotechnology (SAINT), Sungkyunkwan University, Suwon 440-746, South Korea
[b] Department of Physics, Sogang University, Seoul 121-742, South Korea
[c] Nanomaterials Research Group, Physics Division, PINSTECH, Nilore, Islamabad, Pakistan

ARTICLE INFO

Article history:
Received 11 August 2012
Received in revised form
29 November 2012
Accepted 2 December 2012
Available online 5 January 2013

Keywords:
Electrodeposition
Ni nanowires
Magnetic properties
Hysteresis loop

ABSTRACT

Segmented wires (Au–Ni–Au) were synthesized by electrochemical deposition. Magnetic study was performed at 6 kOe field applied parallel to the wire long axis at 300 K and 2 K. Coercivity (H_c) and saturation magnetization (M_s) as a function of segment length (l) were constant for longer l ($5 \leq l \leq 10$ μm) at 300 K and 2 K. However, a peak in H_c was observed for $l=2.4$ μm at 300 K, whereas a decrease in H_c was found for shorter l. M_s followed a decreasing trend with decreasing segment length from 2.4 μm to 200 nm.

1. Introduction

From the application point of view, nanoscale magnetic materials have attracted considerable attention in recent years. Their applications are typically in electronics, magnetic, and biomedical fields [1,2]. Nanowires are synthesized by a variety of techniques including wet chemical solution, nanolithography, physical vapor phase epitaxy, laser ablation, molecular beam epitaxy, and electrochemical deposition of metals into the pores of templates such as in the case of porous anodized alumina oxide or polycarbonate [3–9]. Electrochemical deposition is the most successful technique for the fabrication of high aspect-ratio magnetic nanowires. High-density polycrystalline sandwiched Au–Ni–Au nanowires can be fabricated by the replication of cylindrical pores of the anodized alumina oxide template (AAO). The nanowires prepared using this technique has potential applications in ultra-high density magnetic storage devices [1]. Compared to the ion-track etched polycarbonate templates, the AAO templates are ideal for their uniformity and high density of porous structures. Moreover, these templates are more suitable for the growth of metallic and multisegment nanowires because they are chemically stable and electrically insulating.

There is considerable interest in magnetism and related phenomena for segmented nanowires used as spintronics materials. The intrinsic properties of these nanowires include shape anisotropy, randomness of anisotropy axes, and inter-wire interactions, which are difficult to interpret and need to be studied in detail. As far as the magnetic properties are concerned, owing to the finite size effects, the spins at the surface play a dominant role in nanowires. These surface spins cause a reduction in saturation magnetization with decreasing size and an enhancement in coercivity and magnetic relaxation effects in these wires. Previous studies on nanoparticles showed [10,11] that, owing to the broken symmetries and exchange bonds at the surface of nanoparticles, the surface spins do not follow the core anisotropy direction and become disordered or canted and this leads to an even higher isotropy than that of the core of the particles. This results in the core–shell nature of the particles where the core is ferromagnetic and the shell is composed of disordered or canted spins. Segmented nanowires are expected to exhibit similar behavior where the cylindrical core of the wires is ferromagnetic, whereas the peripheral surface of the cylinder is disordered. Moreover, shape anisotropy also plays a dominant role in segmented nanowires.

In this paper, we report on the fabrication and segment length-dependent magnetic properties of Au–Ni–Au nanowires at room temperature and 2 K. Morphological and compositional analyses were performed using scanning electron microscopy (SEM), transmission electron microscopy (TEM), and x-ray diffraction (XRD). On the other hand, magnetic analysis was performed using a superconducting quantum interface device (SQUID) at an applied magnetic field of 6 kOe. For structural characterization, the nanowires were detached from the templates, whereas for

* Corresponding author. Fax: +82 31 299 4618.
E-mail address: ghkim@skku.edu (G.-H. Kim).

0022-4596/$ - see front matter © 2013 Elsevier Inc. All rights reserved.
http://dx.doi.org/10.1016/j.jssc.2012.12.001

magnetic measurements, the wires were left embedded in the templates.

2. Material and methods

In the present work, we synthesize Au–Ni–Au nanowires having a diameter of 100 nm and a thickness of approximately 13 mm by constant voltage electrochemical deposition into the pores of AAO templates. Electrochemical deposition was performed using a three-electrode DC cell setup. A platinum wire and Ag/AgCl were used as the counter and reference electrodes, respectively. The AAO template with a coated Ag layer on the rear was used as the working electrode. In order to use the AAO template as the working electrode, a thin silver (Ag) layer with a thickness of ~2 μm was evaporated by an electron beam evaporator. For the uniformity of cathode surface a thin sacrificial Ag layer with a thickness of ~2 μm was electrodeposited by applying a constant potential of −0.95 V [12]. Silver plating solution was used for the deposition of the sacrificial layer (~2 μm thick), whereas gold plating solution was used for the growth of Au segments, and Ni sulfate solution was used for the growth of Ni segment.

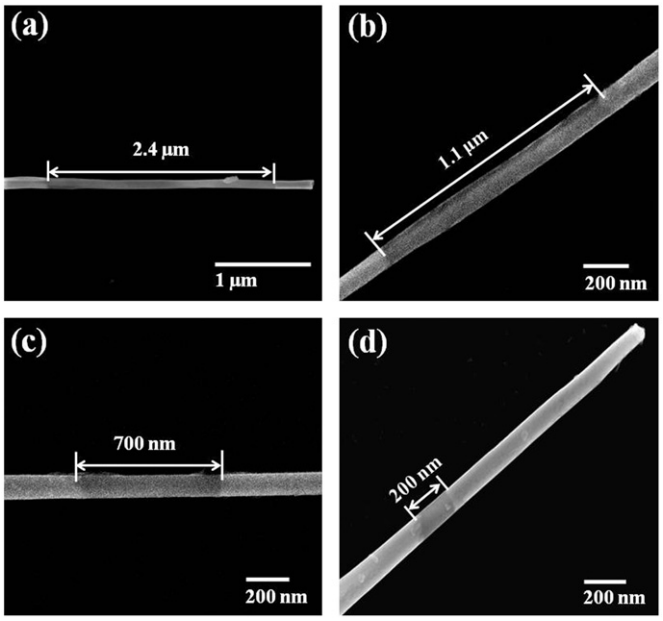

Fig. 1. SEM images of Au–Ni–Au nanowires with Ni segment sandwiched between two gold segments. The length of the Ni segment varies: (a) l=2.4 μm, (b) l=1.1 μm, (c) l=700 nm, and (d) l=200 nm.

The wires were fabricated by keeping the DC voltage (−0.95 V) constant during the entire process and the length of nanowires was adjusted by controlling the deposition time. Gold on both sides was grown in order to control the nickel segment-length up to few nano-meters. The Au segment length was fixed at both ends, whereas the Ni segment length was varied from 10 μm to 200 nm. After the fabrication process, the templates were kept in nitric acid for 15 min to remove the Ag layer used before the deposition. The AAO templates were dissolved in 3 M NaOH solution for 40 min to detach the wires from the templates. In order to get clean nanowires from NaOH, the samples were washed with deionized water 3–4 times by centrifugation and then separated by ultrasonication. For structural analysis, the clean nanowires were dispersed on a silicon wafer and then dried at 120 °C for 20 min. Further details of the synthesis are given in Ref. [13].

The morphology and composition of the samples were investigated using SEM, TEM, energy dispersive x-ray spectroscopy (EDX), and XRD. Magnetic hysteresis loops of the samples with different Ni segment lengths were measured at room temperature (300 K) and at a low temperature (2 K) using a SQUID at an applied field of 6 kOe.

3. Results and discussion

The SEM images of the wires with different Ni segment lengths are shown in Fig. 1(a)–(d). Fig. 1(a) shows the 2.4 μm long Ni segment that is sandwiched between the two gold segments. Fig. 1(b) shows the Ni segment of length 1.1 μm, whereas Fig. 1(c) and (d) shows Ni segments with lengths 700 nm and 200 nm, respectively. The diameter of the wires, which is approximately 100 nm, is clearly seen in the SEM images. The x-ray diffraction pattern of the wires, obtained after dispersion on the silicon wafer, is shown in Fig. 2(a). The wires are liberated from their hosting template by dissolving the template in NaOH and then cleaning by deionized water. Substrate peaks are marked by the asterisk symbol. The peaks in the XRD pattern indicate that the fabricated nanowires are composed of nickel and gold with no extra impurities in the nanowires. XRD analysis confirms the pure-phase crystalline nature of the nanowires. Fig. 2(b) shows the EDX of the nanowires with Si and O peaks of the wafer used for dispersion of the nanowires. Thus, both XRD and EDX results confirm the presence of Ni and Au, whereas the SEM images confirm that Ni is sandwiched between the two gold segments.

Magnetic characterization of the as-fabricated nanowires was performed using a SQUID at 300 K and 2 K. Fig. 3 shows the magnetization hysteresis $M(H)$ loops of three different samples with Ni segment lengths of 10 μm, 2.4 μm, and 200 nm at 300 K and 2 K. The field is applied along the wire's long axis. In our

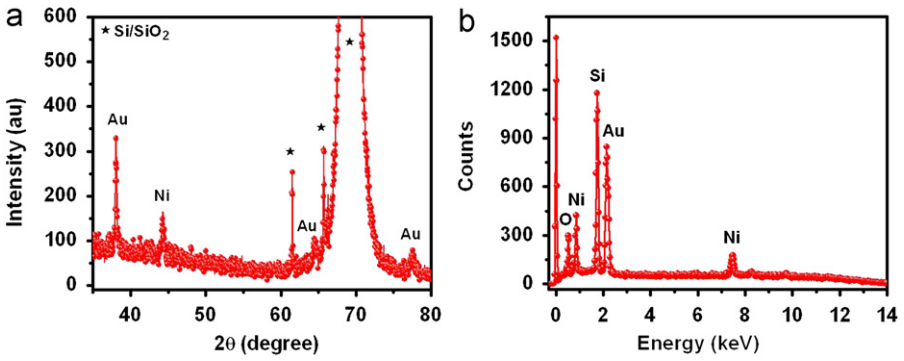

Fig. 2. (a) X-ray diffraction pattern of Au–Ni–Au nanowires confirm crystalline nature of Ni and Au. (b) Energy dispersive x-ray spectroscopy reveals sharp peaks of Au and Ni showing the composition of the nanowires without any impurity peaks.

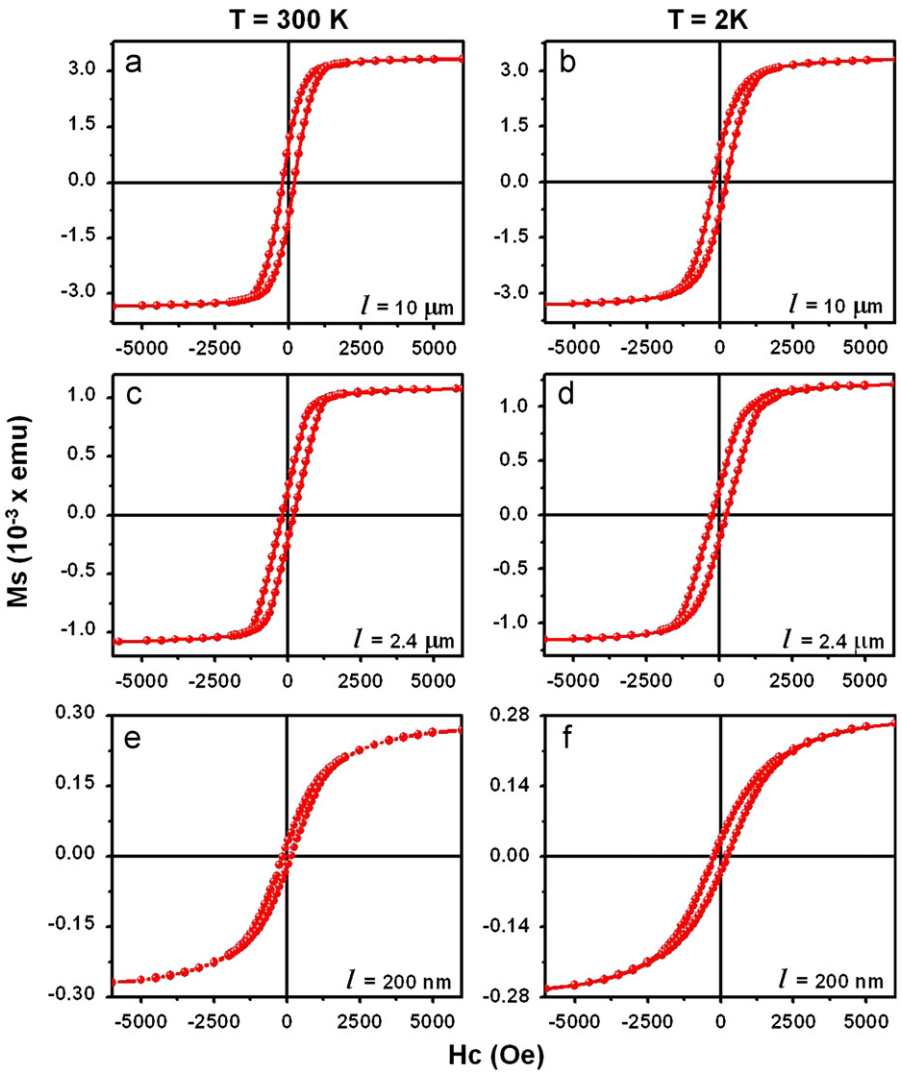

Fig. 3. Magnetic hysteresis curves of Au–Ni–Au nanowires recorded at two different temperatures, 300 K and 2 K for various Ni segment lengths (l). (a) $l=10$ μm at 300 K, (b) $l=10$ μm at 2 K, (c) $l=2.4$ μm at 300 K, (d) $l=2.4$ μm at 2 K, (e) $l=200$ nm at 300 K, and (f) $l=200$ nm at 2 K under an applied field of ± 6 kOe for the wires embedded in AAO templates.

nanowires, it is expected that the anisotropy lies parallel to the wire long axes. Therefore, the field is applied along this direction to get maximum magnetic properties. Fig. 3(a) shows the $M(H)$ loop of Au–Ni–Au nanowires with a Ni segment length of 10 μm obtained at room temperature under an applied field of 6 kOe. The $M(H)$ loops clearly show the ferromagnetic nature of the wires at room temperature, which is attributed to ferromagnetic Ni sandwiched between the two gold segments. Fig. 3(b) shows the hysteresis loop for the 10 μm long Ni segment at low temperature (2 K). Fig. 3(c) shows the room temperature $M(H)$ curve of the nanowires embedded in the AAO template with the 2.4 μm long Ni segment obtained at an applied field of 6 kOe. While the low-temperature hysteresis loop of the same nanowires with the 2.4 μm long Ni segment is shown in Fig. 3(d), the $M(H)$ loops of nanowires with 200 nm long Ni segments at 300 K and 2 K are shown in Fig. 3(e) and (f), respectively. For all these measurements, the wires are embedded in the AAO template and the field is applied in a direction parallel to the wire's long axis.

The plot of coercivity as a function of the Ni segment length (l) at 300 K and 2 K is shown in Fig. 4. The figure shows that there is no variation in H_c for longer Ni segments (10 μm–5 μm) at these temperatures. We consider that the behavior of longer Ni segments ($\geq$ 5 μm) is similar to that of bulk nickel. In our case, the coercivity of the nanowires is ~197 Oe; this is higher than the coercivity (100 Oe) of the bulk Ni at room temperature similar to the case of nanoparticles [14,15]. The high coercivity as compared to the bulk Ni is due to the shape anisotropy, which is parallel to the wire-long axis in the larger Ni segments. Moreover, the surface effects play an important role in case of the nanowires, in which the overall anisotropy energy of the system is high. If we decrease the Ni segment length further (below 5 μm), the coercivity increases continuously and attains a value of 207 Oe for $l=2.4$ μm; however, at a low temperature (2 K), the coercivity increases to 250 Oe for $l=1.1$ μm. It is worth noting that the coercivity at 2 K is higher than that at 300 K in this case; this difference can be interpreted by considering the thermal activation model for the nanostructured materials. If we consider that our segmented nanowires are composed of bead-like structures of nanoparticles each of 100 nm diameter. Then at low temperatures, the anisotropy of nanostructured materials may strongly depend on the temperature according to Kneller's law as follows [16,17]:

$$H_C = H_o\left[\left(1-\frac{T}{T_B}\right)^{1/2}\right] \quad (1)$$

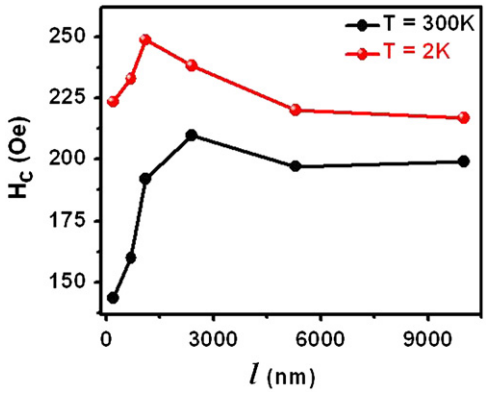

Fig. 4. Plot of coercivity as a function of Ni segment length (l) in the range 10 μm–200 nm at 300 K and 2 K.

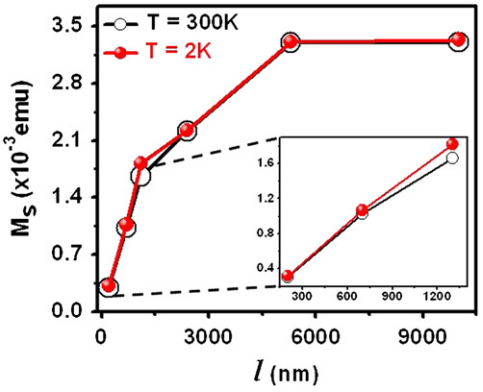

Fig. 5. Magnetization saturation plotted as a function of Ni segment l (10 μm–200 nm) at 300 K and 2 K. Inset shows the enlarged M_s vs. l for small Ni segments (1.1 μm–200 nm).

where H_o is the coercivity at 0 K that can be obtained by extrapolating the H_c versus T curve to the field axis and T_B is the blocking temperature of the nanostructured materials. However, in case of nanowires other effects such as the intrinsic properties of the wires including shape anisotropy, randomness of anisotropy axes, and inter-wire interactions also influence the thermal dependence of coercivity of the samples [18]. However, the dominant factor may be the variation of the shape anisotropy that can affect the coercivity of the nanowires as a function of l. Therefore, the peak in the H_c-segment length (l) curve at 2 K is observed at a length that is relatively shorter (l=1.1 μm) than that at 300 K (Fig. 4). Fig. 4 shows that if we decrease further the Ni segment length, H_c goes on decreasing, which can be attributed to the lower Ni content in the segment sandwiched between the two Au segments. For the shorter Ni segment length (200 nm), the coercivity is minimum (144 Oe), as shown in Fig. 4. To explain the effect of Ni segment length on H_c we consider the shape anisotropy that is weakened as the length of Ni segment is decreased. In this case, owing to the deformation of the cylindrical shape of the Ni segment, the anisotropy direction may not remain parallel to the wire-long axis. For the lengths above the maximum (i.e. $l > 2.4$ μm) the shape anisotropy explains the change in coercivity with l, while below the maximum, the shape anisotropy is not that high and the magnetocrystalline anisotropy starts to play dominant role, producing the domain walls along the nanowires that reduces the coercivity of the wires.

To investigate how the saturation magnetization responds to change in the Ni segment length l, we refer to Fig. 5 that shows that the saturation magnetization is almost constant from 10 μm to 5 μm. However, below this value, M_s decreases almost linearly with the decrease in the length of Ni segment as shown in the inset of Fig. 5. The longer Ni segments result in the higher ferromagnetic Ni contents sandwiched between the Au segments, which result in the high saturation magnetization. Whereas the smaller values of l result in the lower Ni contents sandwiched between the two Au segments causing the lower saturation magnetization values in the nanowires.

4. Conclusions

Multi-segment nanowires (Au–Ni–Au) have been synthesized by electrochemical deposition in AAO templates. Structural analysis confirmed the successful formation of pure crystalline nanowires with a diameter of 100 nm. Magnetic studies with various Ni segment lengths (l) showed that coercivity (H_c) and saturation magnetization (M_s) at 2 K are higher than the corresponding values at 300 K; this difference in values is attributed to the enhanced anisotropy of the system at low temperature. The variation in H_c with the length of Ni segments was attributed to the bulk like behavior of the nanowires (10 μm–5 μm), whereas the decreasing trend in H_c for the shorter Ni segments (below the peak) is attributed to the deformation of the shape anisotropy in the wires. The plot of M_s versus l follows a constant trend for l ranging from 10 μm to 5 μm followed by a decreasing trend in M_s for l below 2.4 μm. This (decreasing) behavior is attributed to the decreasing magnetic content (i.e. Ni) sandwiched between the two nonmagnetic (Au) segments in the nanowires.

Acknowledgments

This research was supported by the World Class University program funded by the Ministry of Education, Science and Technology through the National Research Foundation of Korea (R32-10204).

References

[1] T.T. Albrecht, J. Schotter, G.A. Kastle, N. Emley, T. Shibauchi, L.K. Elbaum, K. Guarini, C.T. Black, M.T. Tuominen, T.P. Russell, Science 290 (2000) 2126–2129.
[2] T. Nautiyal, T.H. Rho, K.S. Kim, Phys. Rev. B. 69 (2004) 193404-1–193404-4.
[3] L. Vayssieres, Adv. Mater. 15 (2003) 464–466.
[4] J. Li, C. Lu, B. Maynor, S. Huang, J. Liu, Chem. Mater. 16 (2004) 1633–1636.
[5] W.I. Park, D.H. Kim, S.W. Jung, G.C. Yi, Appl. Phys. Lett. 80 (2002) 4232–4234.
[6] A.M. Morales, C.M. Lieber, Science 279 (1998) 208–211.
[7] Y.W. Heo, V. Varadarajan, M. Kaufman, K. Kim, D.P. Norton, Appl. Phys. Lett. 81 (2002) 3046–3048.
[8] M. Tian, J. Wang, J. Kurtz, T.E. Mallouk, M.H.W. Chan, Nano. Lett. 3 (2003) 919–923.
[9] Q. Xu, L. Zhang, J. Zhu, J. Phys. Chem. B. 107 (2003) 8294–8296.
[10] H. Kachkachi, M. Nogues, E. Tronc, D.A. Garanin, J. Magn. Magn. Mater. 221 (2000) 158–163.
[11] M. Respaud, J.M. Broto, H. Rakoto, A.R. Fert, Phys. Rev. B 57 (1998) 2925–2935.
[12] N.V. Hoang, S. Kumar, Gil-Ho Kim, Nanotechnology 20 (2009) 125607-1–125607-9.
[13] S. Ishrat, K. Maaz, C. Rong, S.H. Kim, M.H. Jung, Gil-Ho Kim, Curr. Appl. Phys. 12 (2011) 65–68.
[14] J.H. Hwang, V.P. Dravid, M.H. Teng, J.J. Host, B.R. Elliott, D.L. Johnson, T.O. Mason, J. Mater. Res. 12 (1997) 1076–1082.
[15] S.W. Jung, W.I. Park, G-Chul. Yi, M. Kim, Adv. Mater. 15 (2003) 1358–1361.
[16] T. Fukui, C. Sakurai, M. Okuyama, J. Mater. Res. 7 (1992) 791–794.
[17] E.F. Kneller, F.E. Luborsky, J. Appl. Phys. 34 (1963) 656–658.
[18] O. Iglesias, A. Labarta, X. Batlle, J. Nanosci. Nanotechnol. 8 (2008) 2761–2780.